Scalable Photochromic Film for Solar Heat and Daylight Management

Meng, Weihao; Kragt, Augustinus J.J.; Gao, Yingtao; Brembilla, Eleonora; van der Burgt, Julia S.; Schenning, Albertus P.H.J.; Klein, Tillmann; van den Ham, Eric R.; Wang, Jingxia; More Authors

DOI
10.1002/adma.202304910

Publication date
2024

Document Version
Final published version

Published in
Advanced Materials

ADVANCED MATERIALS
www.advmat.de

Scalable Photochromic Film for Solar Heat and Daylight Management

Weihao Meng, Augustinus J. J. Kragt, Yingtao Gao, Eleonora Brembilla, Xiaowen Hu, Julia S. van der Burgt, Albertus P. H. J. Schenning, Tillmann Klein, Guofu Zhou, Eric R. van den Ham, Longfei Tan, Laifeng Li, Jingxia Wang, and Lei Jiang*

The adaptive control of sunlight through photochromic smart windows could have a huge impact on the energy efficiency and daylight comfort in buildings. However, the fabrication of inorganic nanoparticle and polymer composite photochromic films with a high contrast ratio and high transparency/low haze remains a challenge. Here, a solution method is presented for the in situ growth of copper-doped tungsten trioxide nanoparticles in polymethyl methacrylate, which allows a low-cost preparation of photochromic films with a high luminous transparency (luminous transmittance T_{lum} = 91%) and scalability (30 × 350 cm^2). High modulation of visible light (ΔT_{lum} = 73%) and solar heat (modulation of solar transmittance ΔT_{sol} = 73%, modulation of solar heat gain coefficient ΔSHGC = 0.5) of the film improves the indoor daylight comfort and energy efficiency. Simulation results show that low-e windows with the photochromic film applied can greatly enhance the energy efficiency and daylight comfort. This photochromic film presents an attractive strategy for achieving more energy-efficient buildings and carbon neutrality to combat global climate change.

1. Introduction

In response to global climate change, achieving carbon neutrality by 2050 is the most pressing task of our society nowadays. To this end, it is of utmost importance and a significant challenge to improve energy efficiency and reduce carbon emissions.[1] Buildings accounted for 34% of global energy demand and 37% of energy-related CO_2 emissions in 2021, while more than 50% of the building energy is spent on cooling, heating and lighting the interior spaces.[2] Continuous high temperatures in the northern hemisphere during the summer of 2022 exacerbated the energy consumption required to cool buildings.[3] Due to radiation heat losses in winter and solar heat gains in summer, windows are considered to be the least energy-efficient part of a building facade.[4–6]

W. Meng, Y. Gao, J. Wang, L. Jiang
CAS Key Laboratory of Bio-inspired Materials and Interfaces Sciences, Technical Institute of Physics and Chemistry
Chinese Academy of Sciences
Beijing 100190, China
E-mail: jingxiawang@mail.ipc.ac.cn

A. J. J. Kragt, E. Brembilla, T. Klein, E. R. van den Ham
Department of Architecture and the Built Environment
Delft University of Technology
Julianalaan 134, Delft 2628 BL, The Netherlands

X. Hu, G. Zhou
Guangdong Provincial Key Laboratory of Optical Information Materials and Technology, Institute of Electronic Paper Displays, South China Academy of Advanced Optoelectronics
South China Normal University
Guangzhou 510006, China

A. P. H. J. Schenning
Laboratory of Stimuli-Responsive Functional Materials & Devices, Department of Chemical Engineering and Chemistry
Eindhoven University of Technology
P.O. Box 513, Eindhoven 5600 MB, The Netherlands

W. Meng, Y. Gao, J. Wang
Center of Material Science and Optoelectronics Engineering, School of Future Technologies
University of Chinese Academy of Sciences
Beijing 101407, China

L. Tan, L. Li
CAS Key Laboratory of Cryogenics, Technical Institute of Physics and Chemistry
Chinese Academy of Sciences
Beijing 100190, China

A. J. J. Kragt, J. S. van der Burgt, G. Zhou
ClimAd Technology
Valkenaerhof 68, Nijmegen 6538 TE, The Netherlands

J. Wang, L. Jiang
Binzhou Institute of Technology
Weiqiao-UCAS Science and Technology Park
Bingzhou, Shandong 256606, China

The ORCID identification number(s) for the author(s) of this article can be found under https://doi.org/10.1002/adma.202304910

DOI: 10.1002/adma.202304910

Nevertheless, windows are increasingly used in the built environment because they provide an open architecture and allow daylight, which is favorable for people's well-being. However, too much daylight can also cause visual discomfort, typically in the form of glare.[7] To improve energy efficiency and visible daylight comfort in buildings, smart windows are becoming of increasing interest. Smart windows can dynamically regulate the solar transmission (T_{sol}), solar heat gain coefficient (SHGC, the percentage of solar radiation admitted through a window, released as heat inside a building), and visible light transmission (T_{lum}) of glazing depending on outdoor weather conditions.[4–6] Especially in climates with fluctuating seasons and weather conditions smart windows can make an impact on a building's performance.

Existing smart window technology typically has the active materials laminated between the glass panes and thus the installation requires the replacement of the original glazing. This makes the installation of smart windows quite costly and hinders rapid implementation. Therefore, a technology that is easily applicable to existing windowpanes will make fast renovations with smart window technology possible, which enhances its potential impact on a carbon-neutral built environment. Over the years, smart windows appeared that operate by switching an electric field (electrochromic)[8–11] as well as smart windows that respond autonomously to changes in outdoor weather conditions, such as temperature (thermochromic)[12–36] and sunlight intensity (photochromic).[37–46] Compared to electrochromic smart windows, thermochromic and photochromic (PC) smart windows are considered a better choice because of their simple structure, passive light modulation, and zero energy input characteristics. Although thermochromic materials are extensively researched, there are some practical restrictions. For instance, the limitation of VO_2-based smart windows[12–21] is the unfavorable color, service stability, and the balance between T_{lum} and solar modulation (ΔT_{sol}).[35] Perovskite-based smart windows[22,23] also face the problems of insufficient environment stability and ΔT_{sol}.[36] Hydrogel-[18–28] and ionic liquid gel-based[30,31] smart windows have garnered considerable interest for their great transparency and effective solar modulation capabilities, but their scattering properties at elevated temperatures make them opaque, which affects the field of view and people's observation of outdoors. Hybridization of different material systems results in better performance, but still has the limitation of scattering[32,33] or ΔT_{sol}.[34] Photochromic smart windows are more advantageous in these factors.

The current preparation of PC smart windows is mainly based on inorganic PC materials, for their passive bleaching process in dark conditions and better durability compared to organic PC materials.[38] Tungsten trioxide (WO_3) is the most intensively studied inorganic PC material due to its excellent reversibility, fast response to light, and high contrast ratios.[47] The current preparation of WO_3-based smart windows is mainly based on the coating of WO_3, requiring expensive magnetron sputtering equipment.[43] Moreover, most WO_3-based PC devices need liquid electrolytes containing redox media, which inevitably degrades the long-term stability due to leakage phenomena.[42] Encapsulating WO_3 with a polymer binder is another approach to prepare WO_3-based smart windows, however, preparing such composite films with high transparency and low haze remains a challenge. Due to the difference in refractive index between the polymer and WO_3 nanoparticles, light is scattered when passing through the composite film, causing the loss of transparency. This can be avoided by reducing the concentration or the size of nanoparticles (to less than one-tenth of the wavelength of incident light ($<0.1\lambda$)) according to Rayleigh's law.[48] A sufficiently high concentration of WO_3 in the polymer matrix is required to ensure high contrast in sunlight modulation of the PC smart window films. Nevertheless, an excessive concentration will also lead to a decrease in transparency due to agglomeration of the nanoparticles. Reducing the size of nanoparticles is the only solution, even if they are not straightforward, since energy-intensive methods such as hydrothermal synthesis,[37] dialysis,[35] or bead milling[39] are needed to be employed.

Here, we describe the fabrication of an all-solid, free-standing flexible photochromic film with high luminance transmittance (T_{lum} = 91%) and low haze (2.46%) by in situ growth of highly dispersed, small-sized Cu-doped WO_3 nanoparticles[49,50] in a polymethyl methacrylate (PMMA) matrix. The prepared PC films exhibit self-adaptive control of sunlight, as solar transmittance of the PC film is modulated with sunlight intensity without additional energy input. The doping of the WO_3 nanoparticles with Cu, increased the speed from the tinted to transparent state, significantly. The great modulation of visible light (ΔT_{lum} = 73%) and solar heat (ΔT_{sol} = 73%, ΔSHGC = 0.5) shows enormous potential for improving indoor daylight comfort and energy efficiency, which is demonstrated by outdoor testing and building model simulations. The PC film can be used as a non-destructive solution for retrofitting existing windows with no additional replacement cost. Furthermore, we show the scale-up of the PC films (30 × 350 cm^2) by blade-coating, which indicates its potential for large-scale application. This PC film demonstrates a solution for smart windows that can be prepared and applied at low cost, which will have a significant impact on achieving more energy-efficient buildings and carbon neutrality to better address global climate change.

2. Results and Discussion

2.1. Fabrication and Characterization of the PC Film

To achieve a highly transparent and low haze PC film, an in situ growth of WO_3 nanoparticles in a PMMA matrix was developed. To do so, a solution of PMMA in dichloromethane (DCM) was mixed with a solution of tungsten chloride (WCl_6) and copper (I) chloride (CuCl) in *N*,*N*-dimethylformamide (DMF). The mixture was poured into a mold and dried to form a film. During the film formation process, WCl_6 is hydrolyzed using H_2O present in the air to produce WO_3 nanoparticles (**Figure 1A**). The low solubility of PMMA in DMF, insolubility of WCl_6 in DCM, and the different boiling points of the two solvents (DCM 40 °C and DMF 153 °C) allows the stepwise PMMA film formation, which means DCM will completely evaporate before the formation of WO_3 nanoparticles. Therefore, the PMMA matrix adjusts the nucleation process by encapsulating the precursors of nanoparticle (WCl_6/CuCl/DMF) and dispersing them in discrete compartments, thus providing control over the particle growth and preventing particle agglomeration. More specifically, in the precursor solution, PMMA chains are discrete and do not penetrate each other in the DCM solvent ocean; as DCM evaporates, the

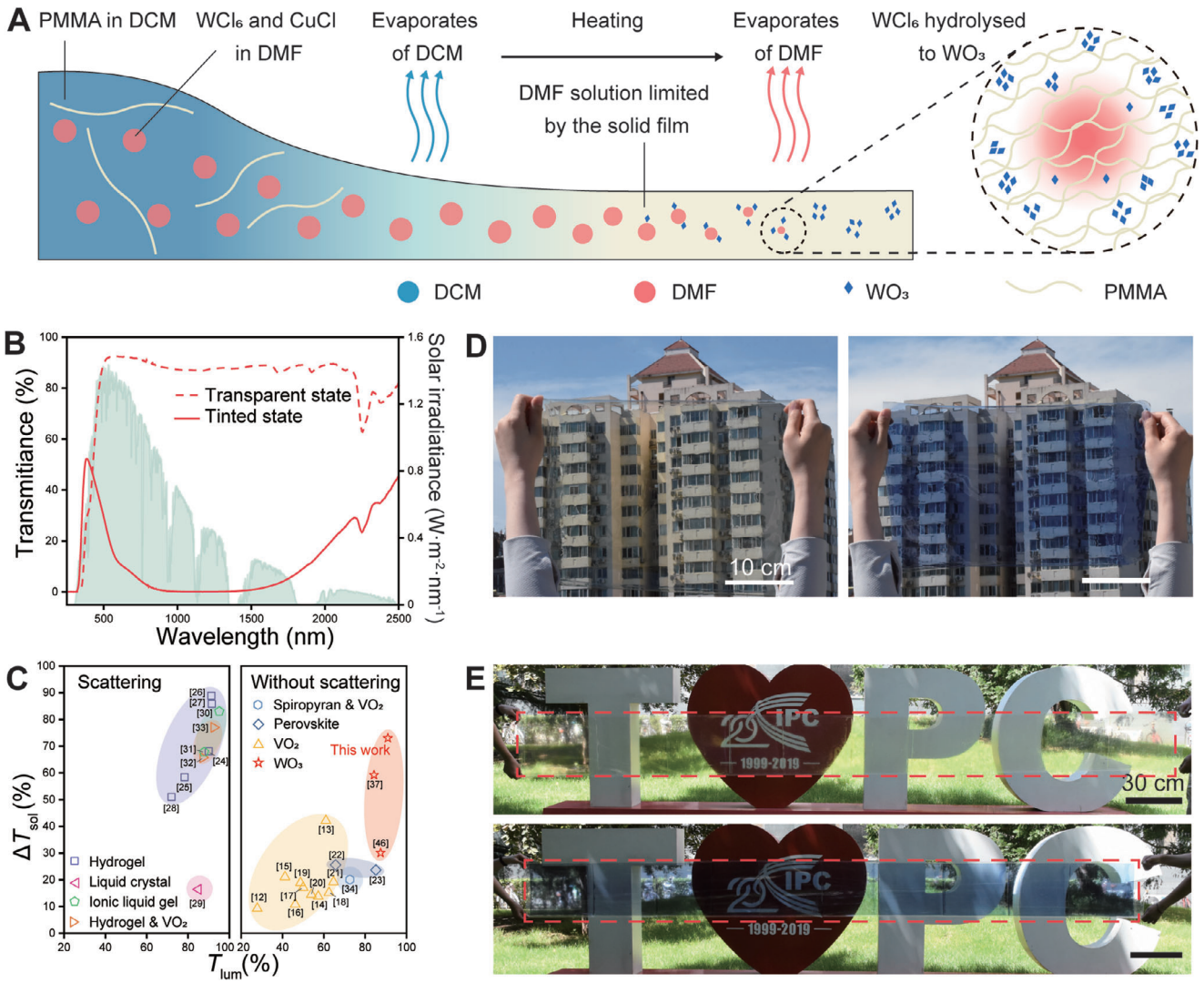

Figure 1. Preparation and working principle of PC film. A) Schematic depiction of the fabrication process for the Cu-W-PC film. The WCl_6/DMF solution and the PMMA/DCM solution were thoroughly mixed and dried in the mold, where the PMMA and Cu-doped WO_3, during which the PMMA and the Cu-doped WO_3 precipitated in steps. B) Transmittance spectra of the Cu-W-PC films at transparent and tinted state (by irradiation with outdoor sunlight for 6 h) against a normalized AM1.5 global solar spectrum (green shadow). C) Summary of T_{lum} and ΔT_{sol} for passively modulated smart windows, which was divided into two types based on the presence or absence of scattering effect. The first type includes hydrogel, ionic liquid gel, and liquid crystal, which has scattering effect and affects the field of view in the tinted state. The second type includes VO_2, perovskite and WO_3 which do not have scattering and has no effect on the field of view. The as-prepared Cu-W-PC film which has superior performance in the second type materials with the highest T_{lum} and ΔT_{sol}. D) Photos of a 30 × 40 cm^2 Cu-W-PC films prepared by the blade-coating method in transparent state (left) and tinted state (right). E) Photos of a 30 × 350 cm^2 Cu-W-PC films on a PET substrate prepared by the blade-coating method in transparent state (top) and tinted state (bottom).

spacing between PMMA chains decreases until they penetrate each other and become entangled. After the DCM completely evaporates, the generation of nanoparticles will be subject to the spatial domain confinement effect of PMMA chains as the DMF evaporates (Figure 1A). Whereas, under the same conditions where the precursor solution does not contain polymers, WO_3 clusters of very large size (micrometer scale) will be obtained (Figure S1, Supporting Information). The ratio of the two solvents is a key factor in achieving this stepwise in situ precipitation (Figure S2, Supporting Information), which determines the particle size of the nanoparticles and thus affects the haze and transparency of the resulting film (Figure S3, Supporting Information). The WO_3 and PMMA composite films prepared with the optimal solvent ratio exhibit extremely low haze (2.48%) as the uniform distribution of nanoparticles (the average particle size of about 1.04 nm) in the film, which can be seen by high-resolution scanning transmission electron microscopy (STEM) images (Figure S4, Supporting Information). In this way, we can simply and efficiently obtain highly dispersed, small-sized nanoparticles in the composite film, instead of the energy-intensive and costly conventional methods (e.g., hydrothermal, dialysis, and bead milling) for preparing composite films of WO_3 nanoparticles and

polymers (Table S1, Supporting Information), which need tight controlling of the reaction parameters to reduce the nanoparticle size and to prevent the agglomeration of nanoparticles. Scanning electron microscopy (SEM) cross section image reveals a thickness of 40 µm and the corresponding energy dispersive spectrometer (EDS) images shows a uniform distribution of nanoparticles throughout the thickness (Figure S5, Supporting Information).

Cu ions[46,51] were introduced into the PC film to accelerate the recovering bleaching process (Cu-W-PC film). The introduction of Cu ions increased the average size of the nanoparticles in the film to 9.34 nm (Figure S4, Supporting Information) and slightly increased the haze of the film to 5.02%. The doping of Cu also introduces a yellowish color (Figure S6, Supporting Information), which can be attributed to an absorption peak around 400 nm of the tetrachloro copper complex ion $[CuCl_4]^{2-}$ formed by the combination of chloride ions and divalent copper ions (Figure S7, Supporting Information). The Cu-W-PC film has good thermal stability up to 130 °C (Figure S8, Supporting Information) and a mechanical strength (tensile stress of 38.7 MPa) slightly lower than that of PMMA film. In addition, it has excellent flexibility for its transmission spectrum does not change after 1000 bending cycles (Figure S9, Supporting Information).

The prepared Cu-W-PC films showed a uniform coloration (tinted state) when irradiated by sunlight and a recovery (bleaching, transparent state) under room light conditions without solar illumination. The Cu-W-PC films in the tinted state exhibit absorption of the majority wavelength ranges present in sunlight (Figure S7, Supporting Information), which is the basis for its regulation of room temperature and daylight comfort. The transmittance spectrum of the Cu-W-PC film in a transparent and tinted state shows a significant solar modulation (Figure 1B). When the Cu-W-PC film is in the transparent state, T_{lum} = 91%, T_{sol} = 85% and SHGC = 0.88. While in the tinted state, the T_{lum}, T_{sol}, and SHGC reduced to 18%, 12%, and 0.38 respectively, which shows an enormous contrast ratio of ΔT_{lum} = 73%, ΔT_{sol} = 73% and ΔSHGC = 0.50 compared to the transparent state. It is worth noting that Cu-W-PC films are without scattering in the tinted state either, that is, the far-field vision through the films remains (Figure S6, Supporting Information). This is an advantage over smart window materials that have scattering properties. Based on the presence or absence of scattering properties, we divide the materials for realizing passively modulated smart windows into two types and summarize their T_{lum} and ΔT_{sol} in Figure 1C. The first type includes hydrogel, ionic liquid gel, and liquid crystal, which have scattering effect and affect the field of view in the tinted state. The second type includes VO_2, perovskite, and WO_3 which do not have scattering and have no effect on the field of view. The as-prepared Cu-W-PC film has superior performance in the second type materials, for it possesses the highest T_{lum} and ΔT_{sol}. The optical characteristics of the PC films in different states are summarized in Table S2, Supporting Information.

Particularly, one of the main advantages of our Cu-W-PC films prepared by the solution method is the ease of manufacturing for large-scale applications. Cu-W-PC film with the size of 30 × 40 cm^2 was prepared by blade-coating, in which the nanoparticles had an average particle size of 1.50 nm, so that it still had high transparency (T_{lum} = 89%) and low haze (2.46%). It still shows photochromism in the presence of sunlight (Figure 1D). For a typical film preparation process, the weight ratio of CuCl, WCl_6, and PMMA in the precursor solution is 0.15:7.5:100, so the concentration of WO_3 nanoparticles in the photochromic film can be calculated as 4.4 wt%, assuming that the WCl_6 is completely converted to WO_3 in the film, while, TGA results showed that the weight ratio of Cu-doped WO_3 nanoparticles in Cu-W-PC film was 3.4 wt% (Figure S8, Supporting Information). When increasing the concentration of CuCl and WCl_6 in the precursor solution, there size of the nanoparticles increases (Figure S10, Supporting Information). However, it is worth noting that a considerable number of nanoparticles with small size (≈1–2 nm) still exist around the larger-sized nanoparticles, indicating that the formation of nanoparticles under these conditions is still subjected to the limiting effect of the polymer. Cu-W-PC flexible film was also prepared on PET substrates with the size of 30 × 350 cm^2 following the same approach (Figure 1E). Also, the preparation cost of Cu-W-PC film is extremely low, with the price of raw materials being only about 0.7 \$ m^{-2}, as shown in Table S3, Supporting Information.

2.2. Photochromic Effect of PC Film

The photochromic effect of the film was further explored by irradiation with UV-light (365 nm) with an intensity of 5 mW cm^{-2} and following the change in transmission over time. The Cu-W-PC film gets a uniform tint over time and its transmittance gradually decreased (**Figure 2**A), where the transmission minimum around 1050 nm (T_{1050nm}) was reduced from 90% to 9% in ≈100 s of irradiation (Figure 2B). After turning off the UV-light source, the Cu-W-PC film recovered to a large extent (T_{1050nm} = 85%) as fast as 20 min in room light and recovered completely to its original state in ≈40 min (Figure 2A,B). Transmittance variations (Figure S11, Supporting Information) and photos (Figure S12, Supporting Information) were recorded for the Cu-W-PC films with different thicknesses prepared with different volumes of the precursor solution in the tinting and bleaching process. The transmittance of the Cu-W-PC film in the tinted state decreases as the thickness increases, which can be explained by Beer-Lambert Law. The thickness of the Cu-W-PC film has little effect on the tinting rate, but significantly affects its bleaching rate. The bleaching rate slows down as the thickness increases. The Cu-W-PC film prepared by the blade coating method with a thickness of about 48 µm demonstrated similar tinting/bleaching processes and optical properties (Figure S13, Supporting Information). It should be noted that for non-doped W-PC film, the photochromic time is shorter (T_{1050nm} dropping from 90% to 9% in ≈40 s of irradiation), but the bleaching process is very slow: it takes >3 days to fully regain its initial transparent state (Figure S14, Supporting Information). In addition, the samples were irradiated with a solar spectrum mimicking lamp (100 mW cm^{-2}). Under these light conditions, the tinting process slowed down because the intensity of UV light irradiated by the sunlight-mimicking lamp is lower than for the UV lamps, while the bleaching process showed a similar trend (Figure S15, Supporting Information). The introduction of Cu ions into the PC film thus significantly accelerates the bleaching process (40 min to bleach completely), which shows sufficient advantages in comparison with reported WO_3-based photochromic smart

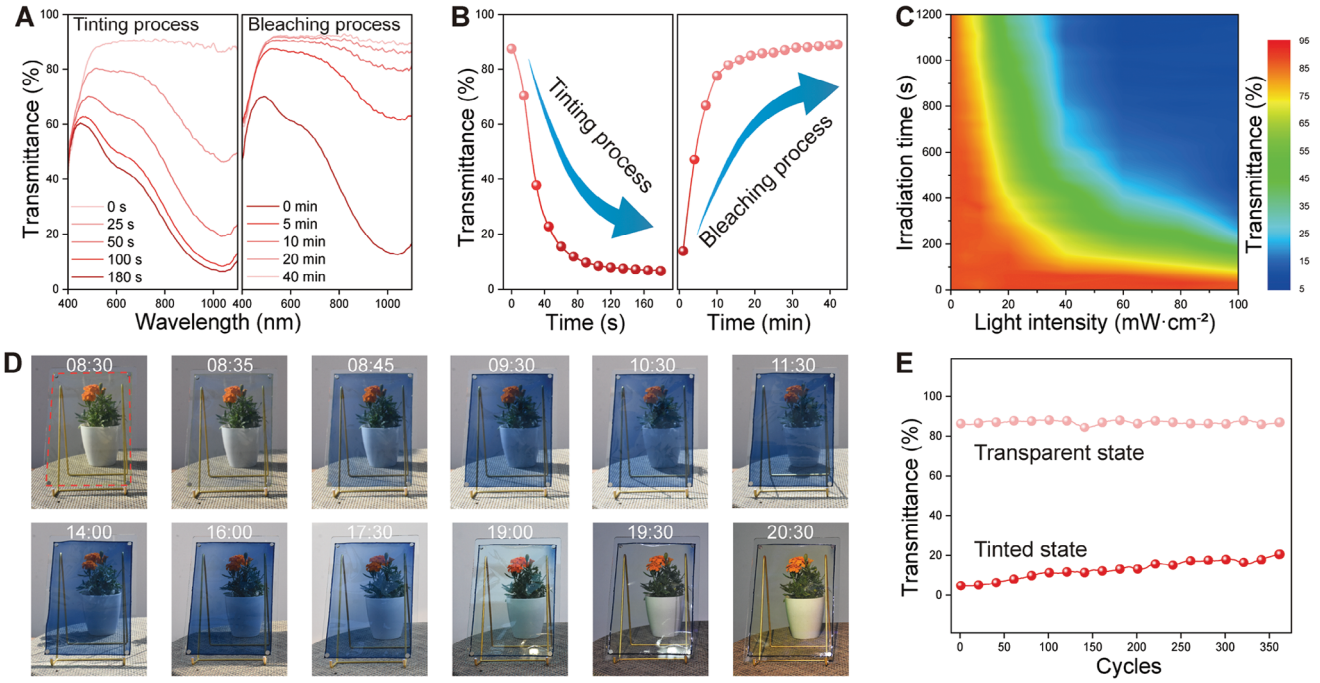

Figure 2. Photochromic effect of PC films. A) Transmittance spectra of the Cu-W-PC films prepared by the mold method during the tinting (irradiation with UV light of 365 nm, 5 mW cm^{-2}) and bleaching process. The transmittance of Cu-W-PC film gradually decreased under UV light, and then the value increased and recovered after turning off the UV-light. B) Transmittance changes of the Cu-W-PC films at 1050 nm during the tinting (left) and bleaching process (right). T_{1050nm} was reduced from 90% to 9% in ≈100 s of irradiation and recovered to a large extent (T_{1050nm} = 85%) in as fast as 20 min in room light, and the value recovered completely to its original state in ≈40 min. C) 2D mapping of the transmittance at 1050 nm of the Cu-W-PC films during the tinting process at varying solar radiation intensity/time, which shows various intermediate tinted states, indicates it is suitable to follow variable sunlight intensities during a day. D) Photographs of the Cu-W-PC films placed outside on a sunny day. E) Transmittance changes of the Cu-W-PC films at 1050 nm during more than 360 cycles of tinting and bleaching.

windows. As a result, we achieved the fastest bleaching process based on the lowest cost doping method, as shown in Table S4, Supporting Information. On sunny days a bleaching time between 20 and 40 min is sufficiently fast as the intensity of daylight diminishes at the end of the day, and the film can easily keep up with changes in daylight. When sunlight intensity decreases more drastically on such a sunny day, such as in the event of a cloud blocking the direct sunlight, the intensity of indirect sunlight is still high and therefore it is still desired for both energy efficiency and daylight comfort to block solar heat and maintain a certain degree of tint. Therefore, 20 to 40 min response time is actually sufficient for practical applications, which is confirmed by glass companies and stakeholders. However, for a broader range of applications it is desired for the shortened bleaching time and optimization.

The speed of the bleaching process can be tuned with the dosage of Cu ions in the system, and the yellow color caused by the absorption of copper doping at 400 nm is also related to the concentration of copper (Figure S16, Supporting Information). We choose to use 20 mol% Cu (with respect to W) in the remaining of this work to have a good balance between a sufficiently fast bleaching process and not clear yellowish color in the transparent state. During the tinting process, when Cu^{2+} is transformed to Cu^{+} the absorption peak at 400 nm decreases and the yellowish color disappears.

The speed of the tinting process is also dependent on the light intensity (Figure 2C, Figure S9, Supporting Information). For example, when the sunlight intensity is 100, 80, 60, 40 mW cm^{-2}, T_{1050nm} drop to 25% requires about 250, 350, 450, 650 s, respectively. When the light intensities >40 mW cm^{-2}, T_{1050nm} drops to about 9%, while at sunlight intensities <40 mW cm^{-2} the Cu-W-PC film maintains various intermediate tinted states, which indicates it is suitable to follow variable sunlight intensities during a day. The PC films were placed outdoors to verify their self-adaptive control to sunlight intensity (Figure 2D and Figure S17, Supporting Information). Clearly, the Cu-W-PC film can change from transparent to tinted state, and then recover to transparent state within the duration of 1 day. The Cu-W-PC film shows good cycling stability (Figure 2E). It can be seen that the contrast between the transmittance at 1050 nm of the Cu-W-PC film in transparent and tinted states slightly decreases after 360 cycles. Figure S18, Supporting Information shows the environmental weatherability of the Cu-W-PC film. The optical properties of Cu-W-PC change little after 7 days of storage under humid-heat conditions and vacuum conditions. Whereas, the contrast between the tinted and transparent states of the Cu-W-PC film decreased significantly after 7 days of placement in the simulated environmental conditions, which matches the results of the cyclic stability tests.

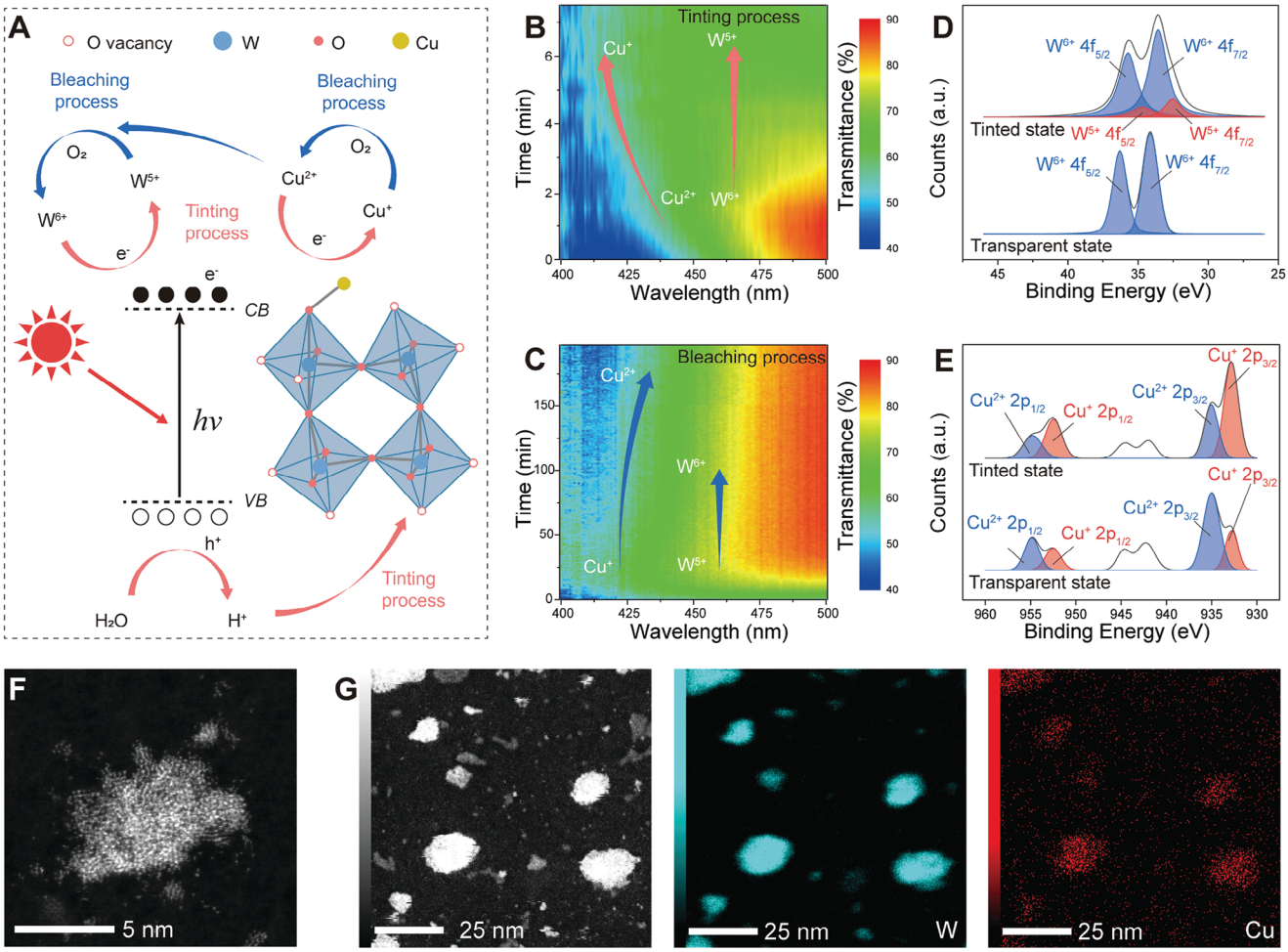

Figure 3. Photochromic mechanism of PC films. A) Schematic illustration of the photochromic and bleaching mechanism of Cu-W-PC film, including the generation of electron and hole pairs in the presence of light, the reduction of Cu^{2+} and W^{6+} by electrons, and their subsequent oxidation by oxygen as an inverse process. 2D mapping result of the transmittance change in B) tinting (irradiation with solar lamp of 100 mW cm^{-2}) and C) bleaching process for Cu-W-PC film. Spectra variations indicate changes in the valence states of W and Cu. XPS spectra of the Cu-W-PC film in tinted state and transparent state for D) W 4f and E) Cu 2p demonstrate the valence change of W and Cu. F) HAADF STEM raw image of Cu-W-PC film demonstrates the amorphous structure of the Cu-doped WO_3 nanoparticle. G) STEM-EDS mapping of W and Cu of the Cu-W-PC film exhibits the distribution of W and Cu in the nanoparticles.

2.3. Photochromic Mechanism of PC Films

For the photochromism of copper-doped WO_3 films, we propose the following mechanism. When the PC films are irradiated with sunlight the WO_3 nanoparticles absorb UV-light and electron-hole pairs are generated (**Figure** 3A). Part of the photogenerated electrons is trapped by oxygen vacancies on the surface of the WO_3 nanoparticles, which reduces W^{6+} to W^{5+}. The abundant oxygen vacancies on the surface result in an increased free charge density, and the free electrons oscillate under an external electromagnetic wave, giving rise to localized surface plasmon resonance (LSPR). This LSPR phenomenon causes a strong absorption of sunlight by the PC films in the tinted state, corresponding to the drastic decrease in the transmittance visible and infrared light range (Figure 3B, right arrow). When introducing Cu^{2+} ions to the film, a fraction of the photogenerated electrons required for the tinting process are consumed by the Cu^{2+}, reducing Cu^{2+} to Cu^{+}, which leads to a slower tinting process. At the same time, the disappearance of Cu^{2+} leads to a decrease in light absorption at 400 nm, corresponding to a higher transmittance (Figure 3B, left arrow). The photogenerated holes are captured by water molecules to generate protons and oxygen. The protons are embedded in the tinted WO_3 nanoparticles to balance the charge of the captured photoelectrons.

Under dark conditions both W^{5+} and Cu^{+} are oxidized by oxygen in the air, forming again W^{6+} and Cu^{2+} returning the film gradually to its initial state, the corresponding transmittance is restored to the initial state (Figure 3C). The oxidation process of W^{5+} is extremely slow, resulting in a slow bleaching process of the W-PC film. In contrast, Cu^{+} is unstable and is very easily oxidized to Cu^{2+} by atmospheric oxygen. The electron transfer from the occupied oxygen vacancies at the surface of the W^{5+} complex to the generated Cu^{2+} ions facilitates the bleaching process of the Cu-W-PC film. In other words,

the redox coupling of Cu^{2+}/Cu^{+} acts as a transfer process of electrons from W^{5+} to O_2. The electron interactions between adjacent W^{6+}, W^{5+}, Cu^{2+}, and Cu^{+} speed up the bleaching process.

To support this proposed mechanism, the PC films were characterized by electron paramagnetic resonance (EPR) and X-ray photoelectron spectra (XPS) measurements. The change in EPR signal demonstrates the trapping of electrons in the oxygen vacancy in the tinted state and the reduction of W^{6+} and Cu^{2+} to W^{5+} and Cu^{+} during the transition from the transparent to the tinted state, respectively (Figure S19, Supporting Information). When comparing the XPS of the Cu-W-PC in transparent and tinted states, peaks of W^{5+} were observed for the tinted state, implying that W^{6+} is partially reduced to W^{5+} by the photogenerated electrons (Figure 3D,E).[52] Also, the change in the ratio of the peak areas[53] of the Cu^{2+} and Cu^{+} signals showed that Cu^{2+} was reduced to Cu^{+}.

The band structure of WO_3 and photoluminescence (PL) spectra of Cu-W-PC are shown in Figure S20, Supporting Information. The PL experiment proved the transfer and separation efficiency of photogenerated charge carriers. The Cu-W-PC film shows drastically lowered PL emission intensity (at 430 nm) than W-PC film, indicating that Cu might effectively facilitate the photogenerated electrons extraction to the Cu active sites. The valence band level 3.25 eV and conduction band (CB) level 0.07 eV span the redox potential of H_2O/O_2 (1.229 V versus normal hydrogen electrode (NHE)) and Cu^{2+}/Cu^{+} (0.153 eV versus NHE), and thus these energy levels can facilitate the photoelectron reduction and atmospheric oxidation reactions for the tinting and bleaching process.

No difference was observed for the X-ray diffraction patterns of PMMA, and Cu-W-PC films, which suggests the amorphous nature of the WO_3 in Cu-W-PC films (Figure S21, Supporting Information). The amorphous structure of WO_3 was confirmed from the HRTEM (Figure S22, Supporting Information) and aberration-corrected high-angle annular dark-field scanning transmission electron microscopy (HAADF-STEM) pictures (Figure 3F). Amorphous WO_3 leads to abundant oxygen vacancies on its surface, which allows photochromic reaction to occur readily even under extremely weak light conditions. STEM-EDS mapping of W and Cu of the Cu-W-PC film shows a uniform distribution and adequate contact between W and Cu in the nanoparticle, which is the basis for electron transfer (Figure 3G). For the undoped WO_3 nanoparticles in W-PC film, it can be seen the distribution of W elements in the nanoparticles, but without Cu elements (Figure S23, Supporting Information). The doping degree of Cu was demonstrated by the corresponding EDS spectra (Figure S24, Supporting Information) (molar ratio of Cu:W ≈ 22:100) and ICP measurements (molar ratio of Cu:W ≈ 27:100) of Cu-W-PC film, which are very close to the molar ratio calculated from the EDS spectra (22:100) and in the precursor solution (20:100).

In dark conditions, both W^{5+} and Cu^{+} are oxidized by oxygen in the air. Therefore, the bleaching rate decreases obviously with increased film thickness, due to the diffusion of oxygen in a thicker PC film (Figure S25, Supporting Information). When the Cu-W-PC films are placed in an oxygen-free environment, the bleaching process does not occur, and the color of the PC films does not change even after 1 h. The bleaching process immediately starts when the Cu-W-PC film is removed from the oxygen-free environment.

2.4. Energy-Saving Potential of PC Films

As the Cu-W-PC film will be able to reduce the temperature of an indoor space, it will also reduce the cooling demand. To explore the energy saving potential of the Cu-W-PC film, the energy consumption of a model office (**Figure 4A**) building equipped with low-e glazing (Figure 4B) with or without Cu-W-PC film was calculated using DesignBuilder. To understand the effect of the photochromic character of the film, calculations of the energy use in case the Cu-W-PC film would be permanently in its tinted state are also included. This was done for two climates with mainly sunny and warm weather conditions all year through (e.g., Guangzhou and Lisbon) and for two climates with more fluctuating weather conditions throughout the seasons (e.g., Beijing and Amsterdam). The steady-state optical properties of the Cu-W-PC film in combination with a single glass plate at various sunlight intensities were measured and included into a low-e window design in DesignBuilder (Figure S26, Supporting Information). The window characteristics at specific sunlight intensities can be found in Table S5, Supporting Information. The energy use on lighting, heating, and cooling of the model office is included and the total energy uses are normalized by setting the energy use for low-e glazing without film to 100% (Figure 4C).

The largest energy-saving potential can be found in warm climates (e.g., Guangzhou and Lisbon). Here annual energy savings of 35.4% and 41.8% are found upon application of the Cu-W-PC film, respectively. In these climates the energy use is dominated by cooling the interior space. As sunlight intensity is high for most of the daytime period throughout the year, the Cu-W-PC film will be mostly in its tinted state, which reduces the need for artificial cooling. Compared to the case of using a permanent tinted window film, the energy saving is slightly reduced in these climates, as the Cu-W-PC film allows some solar heat under lower sunlight intensity conditions (e.g., during mornings, evenings, and cloudy moments). In climates with larger seasonal weather changes (e.g., Amsterdam and Beijing) potential energy savings of 17.9 and 27.6% are calculated, respectively. In these climates, heating in winter also contributes significantly to the annual energy use (Figure 4D). Solar heat rejection during winter days causes an additional energy use for heating. In the case of a permanent tinted window film, this effect is large and even results in an increasing annual energy use of 2.8% for the case of Amsterdam. When using the Cu-W-PC film this effect is also present, but much smaller compared to the use of a permanent tinted window film, resulting in a net annual energy saving. This can be attributed to the transmission of solar heat by the Cu-W-PC film during conditions of lower sunlight intensity in winter, which will be blocked in case of a permanent solar heat rejection film. When a building is equipped with double or single glazing (Figure S27, Supporting Information), thus having less insulating properties, the energy used for heating becomes larger, while that of cooling becomes smaller, which reduces the impact of the Cu-W-PC film. Nevertheless, still significant energy savings can be expected

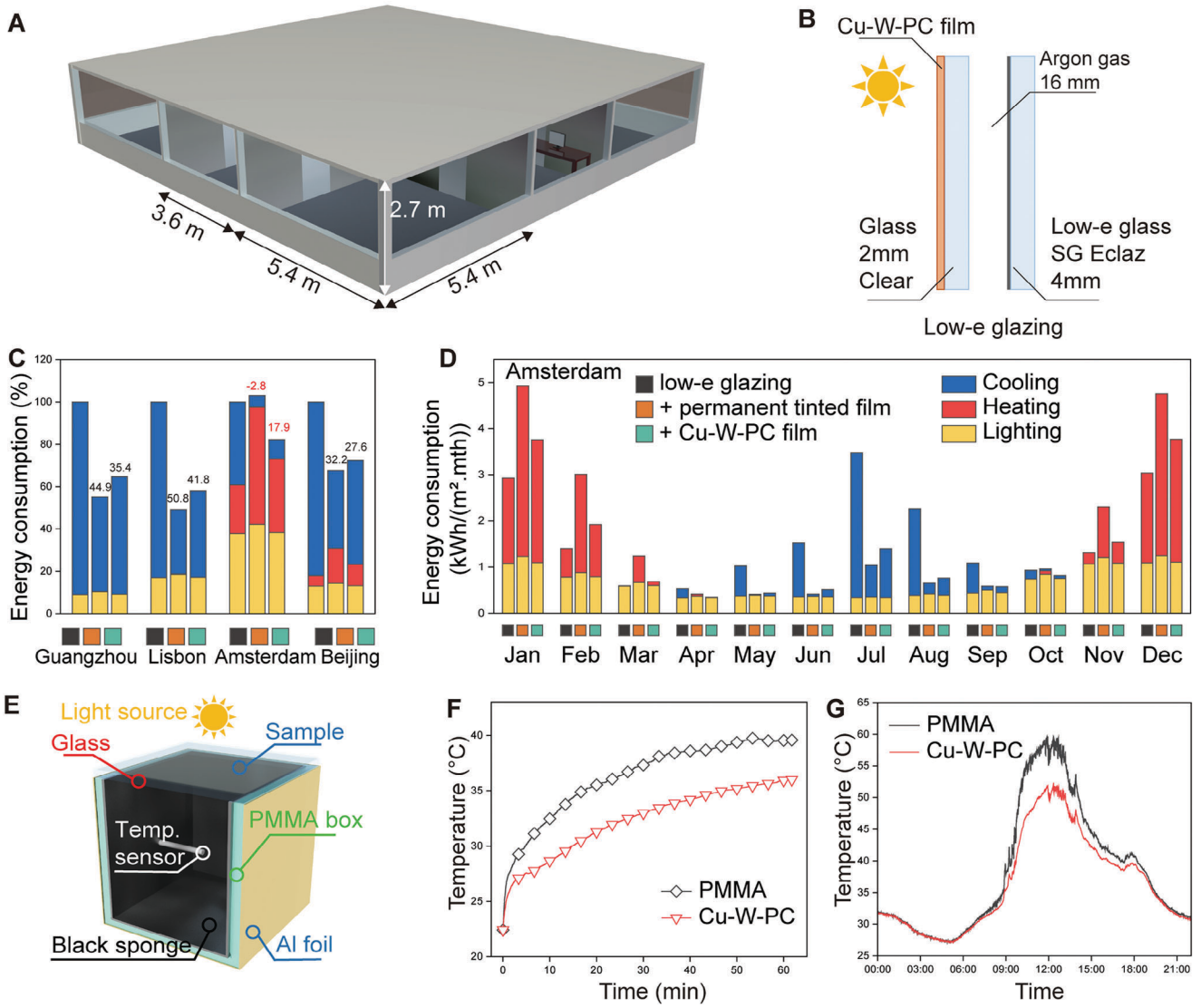

Figure 4. Impact of the PC films on indoor temperature and simulation of energy consumption in a model office building. Representation of the A) office and B) glaze model used to evaluate the energy-saving potential of the Cu-W-PC film. C) Calculated and normalized annual energy use for lighting, heating, and cooling for different cities. D) Calculated monthly energy use in Amsterdam. E) Schematic representation of the model house. Temperature curves for the model houses under the F) simulated sunlight 100 mW·cm^{-2} for 1 h and G) field test for 1 day.

ranging between 12.3% and 31.7% (Figure S28, Supporting Information) in warm climates (e.g., Guangzhou and Lisbon). However, in climates like Amsterdam and Beijing, it is recommended that Cu-W-PC films be used in combination with well-insulated glass if only the energy performance of the building is to be considered.

To validate the effect of solar heat rejection, and thus the potential to save energy on cooling loads, by the PC films in real-life the indoor temperature of a model house was monitored (Figure 4E). Two samples (Cu-W-PC and PMMA films) were attached to a 2 mm thick glass plate and placed on the windows of two identical model houses. The model houses were made of acrylic boxes with a dimension of 15 × 15 × 15 cm^3 and sealed with thermal insulation materials (the interior is covered with black sponge and the exterior is wrapped with Al foil). The air temperature of the inner space is monitored when irradiating with solar radiation of 100 mW cm^{-2} (Figure 4F). A 4 °C reduction is achieved for the model houses equipped Cu-W-PC film compared to the control experiment with a PMMA film without the photochromic nanoparticles. In addition, the same model houses were placed outside on a sunny summer day in Beijing while monitoring the indoor temperature (Figure 4G). The maximum indoor air temperature of the model houses equipped with the Cu-W-PC (52.3 °C) films was >7.4 °C lower than that of the model house with PMMA (59.7 °C), which confirms the solar heat rejection effect induced by the PC films, underlying the reduction of cooling energy loads in the DesignBuilder simulation.

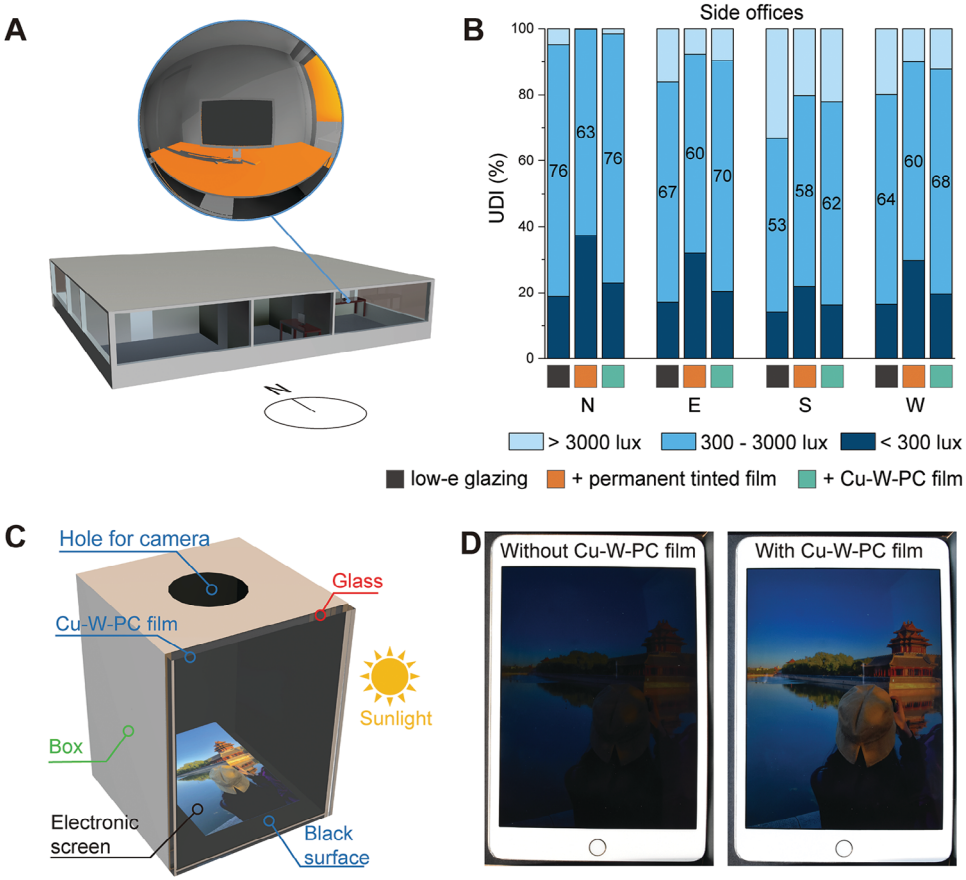

Figure 5. Simulation of useful daylight illuminance (UDI) and daylight glare probability in a model office building. A) Representation of the model office used for daylight visual comfort analysis including two simulated desk positions within the model office building and the field of view from one of the desks sitting positions, highlighting sources of glare at a given time. B) UDI for side rooms' orientation (N for North, E for East, S for South, W for West) of the model office located in Amsterdam equipped with low-e glazing without film, with a permanent tinted film and with the Cu-W-PC film. C) Schematic representation of the test box to show the visibility of an electronic screen. D) Photos of the electronic screen at high sunlight intensity without and with the Cu-W-PC film.

2.5. Impact of the PC Films on Daylight Visual Comfort

In addition to lowering the indoor temperature and saving energy, the Cu-W-PC film also impacts the daylight visual comfort. This was explored by simulating the daylight illuminance level of the same office floor model and climates as used for the energy use calculation but using the Radiance command suite (**Figure** 5A).[54] The average illuminance levels of each room at a specific moment during occupied hours throughout the year were calculated. These were categorized into three groups (Figure S29, Supporting Information), referred to as useful daylight illuminance (UDI) categories:[55] "too dark" (<300 lux), "comfortable" (between 300 and 3000 lux), and "too bright" (>3000 lux). The percentage of time in each UDI-category is plotted for each room of the office model in Amsterdam (Figure 5B and Figure S30, Supporting Information). This analysis shows that implementation of the Cu-W-PC film increases the time of "comfortable" daylight illuminance level compared to the situation without film for almost all the room orientations. The times at which the rooms are "too bright" (>3000 lux) are reduced as the Cu-W-PC film will be in its tinted state (at these moments of high outdoor sunlight intensity). The times at which the rooms are "too dark" (<300 lux) are almost the same, as the Cu-W-PC film will be in its transparent state like a regular window at these moments of low outdoor sunlight intensity. When comparing the Cu-W-PC film with a permanently tinted film, the Cu-W-PC film increases the time of "comfortable" illuminance as well in side offices having just one window (Figure 5B). Although, the permanent tinted film is more effective in reducing the moments of too high illuminance (>3000 lux), a permanent tinted film causes the rooms to be "too dark" (<300 lux) more often compared to the Cu-W-PC film. The corner offices having two windows are "too bright" for much of the occupied time. For these office spaces, it can be more beneficial to install a permanently tinted film when considering daylight visual comfort (Figure S28, Supporting Information). This effect is also seen in other climates (Figure S31, Supporting Information).

The impact of the Cu-W-PC film on daylight visual comfort is also studied by daylight glare probability (DGP) analysis. The DGP index is used to express whether glare is commonly experienced by people as "intolerable" (>0.45), "disturbing" (0.40 – 0.45), "perceptible" (0.35–0.40), or "imperceptible" (<0.35).[56] In

this study, two desk positions close to the window in the south and south-east room of the model office are analyzed and the DGP index during occupied hours (8 AM to 6 PM) over the year for a person sitting at one of the desks is calculated (Figure 5A). Again, the situation of the model office equipped with low-e glazing without film is compared with the situation in which a permanent tinted film or the Cu-W-PC film is applied to the glazing. For all climates, it is found that the Cu-W-PC film improves the glare comfort level over the year, as the DGP index is more frequently in the "imperceptible" range and less in the "intolerable" range (Figure S32, Supporting Information). As the Cu-W-PC film tints at moments of high sunlight intensity the film cuts off annoying glare. Zooming in on the DGP indices throughout the days over the year reveals that for the south-east office, the Cu-W-PC film improves glare comfort mostly during morning hours, whereas for the south office glare comfort is mostly enhanced around the afternoon hours (Figure S33, Supporting Information). This finding is expected considering the trajectory of the sun coming up in the east and being positioned south in the afternoon. The DGP analysis also reveals that a permanent tinted film would improve the glare comfort level more compared to the Cu-W-PC film. This can be expected as such film will also be in a fully tinted state at conditions of annoying glare during intermediate sunlight intensities. However, as revealed with the UDI analysis, this might also result in the room in general to be too dark (Figure 5B). Considering the overall daylight visual comfort level compared to a permanent tinted film, the Cu-W-PC film cuts off annoying glare at moments this is most needed, but also allows daylight at moments of lower sunlight intensity to prevent a room from being too dark.

To validate the improvement of daylight comfort in practice, a test box was designed in which an electronic screen was placed (Figure 5C). Without the Cu-W-PC film, the image on the electronic screen cannot be seen clearly under strong sunlight conditions (Figure 5D, right). When the Cu-W-PC film is placed on the glazing of the box, the image on the screen becomes well visible, as the film tints and provides a better contrast between the screen and its surroundings (Figure 5D, left).

3. Conclusion

The as-prepared PC film has an extremely low fabrication cost and can be installed cost-effectively to renovate any existing window. The PC film demonstrates an excellent solar heat (ΔT_{sol} = 73%, ΔSHGC = 0.5) and daylight regulation (ΔT_{lum} = 73%), while being almost invisible in the transparent state (T_{lum} = 91%). The PC films can autonomously regulate a comfortable visible daylight entrance, cut off annoying glare when needed, and reduce indoor temperature at moments of high sunlight intensity. Simulations show that our PC film provides significant energy savings when being applied to different glazings in various climates. For example, in warm areas, such as Lisbon, low-e windows with PC film reduced the annual energy consumption of buildings by 42%, while in climates with significant summer and winter conditions, such as Amsterdam, energy efficiency was significantly higher compared to permanent tinting schemes, and in all areas, the implementation of photochromic films increased "comfortable" daylight illuminance level and "imperceptible" glare compared to the situation without film. Moreover, a large-area PC film has been prepared by blade-coating, which indicates the potential for large-scale applications of the PC film. The PC film just needs to be attached to the outer surface of the existing windows with a transparent adhesive layer between the film and the glass. Additionally, the film may be implemented at the side of a glass pane facing the cavity of a double-pane window. In this case, the film should be applied during the assembly of the glazing unit. Both integration options will be investigated in future work.

4. Experimental Section

Materials: Tungsten chloride, copper (II) chloride, and 1,2-dichloroethane were purchased from Aladdin. DCM and DMF were purchased from Sinopharm Chemical. PMMA (heat stability injection grade) was purchased from Shanghai Macklin. 30% Hydrogen peroxide (30%, Analytical Reagent) was purchased from Xilong Scientific Co., Ltd.

Preparation of the PC Films by Mold Method: 0.3 g of tungsten chloride (WCl_6) and 60 µL of 30% hydrogen peroxide (H_2O_2) were dissolved in 1.5 mL of DMF and stirred for 2 h at room temperature to form a solution. H_2O_2 acts as an oxidizing agent and leaves the newly prepared film in the transparent state. 4 g of PMMA was dissolved in 50 mL of DCM and stirred for 2 h at room temperature. The two solutions were mixed and stirred for 2 h to obtain a precursor solution for the PC films. The precursor solution was poured into an A4 size quartz tray and dried in an oven at 40 °C for 1 h. After demolding the A4 size PC film was obtained. W-PC film with different solvent ratios was obtained by varying the amount of DMF. 0.5, 0.75, and 1 mL DMF corresponds to DMF:DCM = 1:100, 1.5:100, and 2:100 W-PC film, respectively. For the Cu-W-PC films preparation, the procedure was the same as above, except that 0.015 g of copper (I) chloride (CuCl) was added to the DMF solution before stirring.

Preparation of the PC Films by Blade Coating Method: A control coater (PF400, Jiangsu LEBO) was used to prepare the PC films with A3 size. 0.6 g of tungsten chloride (WCl_6) and 0.03 g of copper (I) chloride (CuCl) were dissolved in 3 mL of DMF and stirred for 2 h at room temperature to form a solution. 8 g of PMMA was dissolved in 16 mL of 1,2-dichloroethane for 8 h at room temperature. The two were mixed and stirred for 1 h at room temperature to obtain a precursor solution for the PC films. Then, the coating was applied using a 200 µm gap, which was pushed forward over the mixture automatically by the coater at 70 °C on the PET or glass substrate surface. The speed of the applicator movement was about 100 mm s^{-1}. And it was placed on the hotplate of the applicator at 70 °C for 30 min to evaporate the solvent. After detaching the coating layer from the substrate, the A3 size PC film was obtained. For the 30 × 350 cm^2 Cu-W-PC films preparation the procedure was the same as above, except that the preparation process was repeated successively by blade coating on a roll of PET substrate.

Illumination Time-Dependent UV–vis-NIR Spectroscopy: The transmission spectra of the PC films were recorded every 0.1 s with an optical fiber coupled spectrometer (USB 2000, Ocean Optics) mounted on the microscope (Olympus, BX51) during the UV light illumination (5 mW cm^{-2}) from the H086-425 and once a minute during the bleaching process.

Light Intensity-Dependent UV–vis-NIR Spectroscopy: The transmission spectra of the PC films were recorded every 30 s for a total of 20 min with the optical fiber-coupled spectrometer under the irradiation of a solar simulator PL-X300DF. The process was repeated by varying the intensity of the solar simulator. The light intensity was calibrated by CEL-NP2000-2(10)A, CEAULIGHT.

Transmission, Reflection, and Absorption UV–vis-NIR Spectroscopy for PC Films in a Defined State: PC films were exposed to outdoor sunlight for 6 h to reach their full tinted state. The spectra of PC films in the tinted or transparent state were recorded with a spectrometer Cary 7000, Agilent with integrating sphere attachment. The haze of the film was obtained utilizing a haze meter (CS-700, Hangzhou CHNSpec). All pictures were obtained by D7200, Nikon.

Morphology of the PC Films: SEM images were obtained by S-4300. TEM images were obtained by HT7700. The high-angle annular dark-field (HADDF) STEM images were obtained by JEM-ARM300F. XPS measurements were accomplished via a photoelectron spectrometer (PHI5000 VersaprobeIII XPS) with an Al Kα radiation source. Electron spin resonance (ESR) spectra were obtained over Bruker E 500 at 108 K with in situ UV irradiation (5 mW cm^{-2}). ICP test was accomplished by ICP-MS:Agilent 7800.

Energy Performance Calculations: To define the glazing characteristics the Cu-W-PC film was placed on a single clear glass plate of 2 mm thick. The transmission and reflection measurements were performed after maintaining various sunlight intensities using a PL-X300DF solar simulator for 30 min allowing the film to reach a steady state. This was done upon increasing and decreasing the sunlight intensity to include hysteresis between the steady-states during the tinting and bleaching process. The steady-state spectra at a certain sunlight intensity were averaged and implemented in the LBNL software Optics6 to define the optical properties at a certain sunlight intensity. The model office was designed in DesignBuilder and the four identical sides of the office were oriented toward the North, East, South, and West. The window-to-wall ratio of the model office was 60%. The floor and ceiling of the office were designed to be adiabatic, to mimic an office space with adjacent building levels. The outdoor walls were medium-weight walls having a *U*-value of 0.25 W m^{-2} K^{-1}. The building was equipped with an LED lighting system having a normalized power density of 2.5 W m^{-2} per 100 lux and was turned on when the illuminance level dropped below 400 lux at a working height of 0.8 m during occupied hours. The HVAC system was based on the "Best practice" template defined in DesignBuilder. The heating system ran on natural gas and had a coefficient of performance (CoP) of 1.0 and was activated when the indoor temperature of a room dropped below 20 °C. For operation schedule, the DesignBuilder template "Office_OpenOff_Heat" was used. The cooling system ran on electricity from the grid and had a CoP of 2.5 and was activated when the indoor temperature rose above 25.5 °C during occupied hours (DesignBuilder template "Office_OpenOff_Cool"). Furthermore, the activity was based on the "Generic Office Area" template defined in DesignBuilder. The model office has an occupation density of 0.111 people per m^2 and operates according to the standard open office occupancy schedule (DesignBuilder template "Office_OpenOff_Occ"). During the operational hours defined by this occupancy schedule office equipment was used with a power density of 11.77 W m^{-2}. During the simulations all modeling parameters, except for the glazing, were kept constant. The low-e coated double glazing with and without Cu-W-PC film was designed within DesignBuilder. For the low-e coated glass plate, the input optical data from Saint-Gobain Eclaz 4 mm were taken from the IGDB database in the LBNL software Window 7.7. Argon 16 mm was chosen as gas filling between the two glass plates. For the reference case without Cu-W-PC film, the second glass pane was defined by the optical properties of the 2 mm glass plate. For the case with Cu-W-PC film, the second glass pane was defined by the optical properties of the 2 mm glass plate with the Cu-W-PC film in its transparent state. An assumption was made that the *U*-value was the same for coated and uncoated glass here, because the emissivity of ordinary glass ($\epsilon = 0.84$) was close to the emissivity of the film ($\epsilon = 0.88$). To introduce the photochromic effect in the calculation, the "window shading" feature was used. Here the optical properties of the second glass pane at various sunlight intensities were defined based on the optical properties determined above. The window shading was controlled by "daylight only" and operated "24/7" to mimic the autonomous working principle of the Cu-W-PC film. For the model calculation each window was provided with a single light-intensity "sensor," so the various windows of the building model operated individually. The weather data files were downloaded from www.climate.onebuilding.org, which provided typical meteorological year datasets for the specific locations, which were then imported into the DesignBuilder model.

Daylight Performance Calculations: To assess indoor daylight access and visual comfort, the same office building geometry, material properties, and weather data files as for the energy calculations were used. The daylight access analysis was performed for all eight office rooms (four corner rooms and four side-lit rooms) and was simulated on a horizontal grid at a height of 0.8 m from floor level. The Radiance 3-phase method[57] was used for the annual performance simulations that produced UDI results, to account for the variable visible transmittance of the photochromic glazing. The correct transmittance was selected based on an irradiance calculation performed with the Radiance 2-phase method,[58] for each individual window at a point placed in the center of the glass and facing outward. The glare analysis was performed with the Radiance evalglare[56] command, which allowed to calculate the DGP metric from a rendered field of view from the position of a building occupant. Two sitting positions were chosen within the case study building: one in the South-East corner room, facing North; and one in the South side-lit room, facing East. In both cases, the height of the occupant's eyes was assumed to be 1.20 m height above the floor and their gaze was fixed on a computer screen placed on the desk in front. To allow for an efficient annual glare evaluation, the vertical illuminance at eye level was precomputed with a higher accuracy simulation run and then provided to evalglare, while the simulation needed to produce a rendered field of view was kept at a lower accuracy and took into account only direct sunlight. As suggested in previous studies,[59] the evalglare threshold method with a threshold value of 2000 cd m^{-2} was adopted for all evaluations.

Statistical Analysis: Haze of the film was tested at five different points in each sample and averaged. The calculated energy consumption for 1 year in Figure 4B was normalized by putting the energy use with low-e glazing without film to 100%.

Supporting Information

Supporting Information is available from the Wiley Online Library or from the author.

Acknowledgements

W.M., A.J.J.K., and Y.G. contributed equally to this work. The authors thank the financial support of the Chinese Academy of Sciences and Dutch research project (1A111KYSB20190072) and National Natural Science Foundation of China (grant nos. 52373001, 51873221, 52073292, 51673270, 21774003, and 51373183).

Conflict of Interest

The authors declare no conflict of interest.

Data Availability Statement

The data that support the findings of this study are available from the corresponding author upon reasonable request.

Keywords

daylight comfort, energy saving, photochromicity, scalability, smart windows, transparency, tungsten trioxide

Received: May 23, 2023
Revised: November 1, 2023
Published online: December 5, 2023

[1] F. Wang, J. D. Harindintwali, Z. Yuan, M. Wang, F. Wang, S. Li, Z. Yin, L. Huang, Y. Fu, L. Li, S. X. Chang, L. Zhang, J. Rinklebe, Z. Yuan, Q. Zhu, L. Xiang, D. C. W. Tsang, L. Xu, X. Jiang, J. Liu, N. Wei, M. Kastner, Y. Zou, Y. S. Ok, J. Shen, D. Peng, W. Zhang, D. Barcelo, Y. Zhou, Z. Bai, et al., *Innovation* **2021**, *2*, 100180.

[2] United Nations Environment Programme, *2022 Global Status Report for Buildings and Construction: Towards a Zero-Emission, Efficient and Resilient Buildings and Construction Sector*, Nairobi, https://globalabc.org/our-work/tracking-progress-global-status-report, **2022**.
[3] H. Saeed Khan, R. Paolini, P. Caccetta, M. Santamouris, *Energy Build.* **2022**, *267*, 112152.
[4] Y. Ke, J. Chen, G. Lin, S. Wang, Y. Zhou, J. Yin, P. S. Lee, Y. Long, *Adv. Energy Mater.* **2019**, *9*, 1902066.
[5] H. Khandelwal, A. P. H. J. Schenning, M. G. Debije, *Adv. Energy Mater.* **2017**, *7*, 1602209.
[6] Y. Zhou, F. Fan, Y. Liu, S. Zhao, Q. Xu, S. Wang, D. Luo, Y. Long, *Nano Energy* **2021**, *90*, 106613.
[7] R. G. Hopkinson, *Appl. Ergon.* **1972**, *3*, 206.
[8] J.-L. Wang, S.-Z. Sheng, Z. He, R. Wang, Z. Pan, H.-Y. Zhao, J.-W. Liu, S.-H. Yu, *Nano Lett.* **2021**, *21*, 9976.
[9] J.-L. Wang, J.-W. Liu, S.-Z. Sheng, Z. He, J. Gao, S.-H. Yu, *Nano Lett.* **2021**, *21*, 9203.
[10] Z. Shao, A. Huang, C. Ming, J. Bell, P. Yu, Y.-Y. Sun, L. Jin, L. Ma, H. Luo, P. Jin, X. Cao, *Nat. Electron.* **2022**, *5*, 45.
[11] J. Chen, Z. Wang, C. Liu, Z. Chen, X. Tang, Q. Wu, S. Zhang, G. Song, S. Cong, Q. Chen, Z. Zhao, *Adv. Mater.* **2021**, *33*, 2007314.
[12] S. Wang, T. Jiang, Y. Meng, R. Yang, G. Tan, Y. Long, *Science* **2021**, *374*, 1501.
[13] X. Li, C. Cao, C. Liu, W. He, K. Wu, Y. Wang, B. Xu, Z. Tian, E. Song, J. Cui, G. Huang, C. Zheng, Z. Di, X. Cao, Y. Mei, *Nat. Commun.* **2022**, *13*, 7819.
[14] N. Shen, S. Chen, W. Wang, R. Shi, P. Chen, D. Kong, Y. Liang, A. Amini, J. Wang, C. Cheng, *J. Mater. Chem. A* **2019**, *7*, 4516.
[15] X. Zhou, Y. Meng, T. D. Vu, D. Gu, Y. Jiang, Q. Mu, Y. Li, B. Yao, Z. Dong, Q. Liu, Y. Long, *J. Mater. Chem. A* **2021**, *9*, 15618.
[16] Q. Xu, Y. Ke, C. Feng, C. Chen, Z. Wen, H. Wang, M. Sun, X. Liu, H. Liu, S. Magdassi, H. Li, C. Huang, Y. Long, *Sol. Energy Mater. Sol. Cells* **2021**, *230*, 111182.
[17] X. P. Zhao, S. A. Mofid, T. Gao, G. Tan, B. P. Jelle, X. B. Yin, R. G. Yang, *Mater. Today Phys.* **2020**, *13*, 100205.
[18] S. Wu, L. Zhou, B. Li, S. Tian, X. Zhao, *Nanomaterials* **2023**, *13*, 2252.
[19] H. Ji, Y. Zhao, M. Lu, J. Tao, Y. Chen, Y. Ou, Y. Wang, Y. Mao, *Ceram. Int.* **2023**, *49*, 22630.
[20] X. Yang, J. Zou, *J. Alloys Compd.* **2023**, *940*, 168868.
[21] J. Liang, Z. Yang, D. Zhang, S. Wang, H. Zhang, W. Tai, *Mater. Today Commun.* **2022**, *33*, 104544.
[22] S. Liu, Y. Li, Y. Wang, K. M. Yu, B. Huang, C. Y. Tso, *Adv. Sci.* **2022**, *9*, 2106090.
[23] S. Liu, Y. W. Du, C. Y. Tso, H. H. Lee, R. Cheng, S.-P. Feng, K. M. Yu, *Adv. Funct. Mater.* **2021**, *31*, 2010426.
[24] Y. Zhou, S. Wang, J. Peng, Y. Tan, C. Li, F. Y. C. Boey, Y. Long, *Joule* **2020**, *4*, 2458.
[25] C. Lin, J. Hur, C. Y. H. Chao, G. Liu, S. Yao, W. Li, B. Huang, *Sci. Adv.* **2022**, *8*, eabn7359.
[26] G. Chen, K. Wang, J. Yang, J. Huang, Z. Chen, J. Zheng, J. Wang, H. Yang, S. Li, Y. Miao, W. Wang, N. Zhu, X. Jiang, Y. Chen, J. Fu, *Adv. Mater.* **2023**, *35*, 2211716.
[27] J. Li, P. Gu, H. Pan, Z. Qiao, J. Wang, Y. Cao, W. Wang, Y. Yang, *Adv. Sci.* **2023**, *10*, 2206044.
[28] S. Wang, Y. Zhou, T. Jiang, R. Yang, G. Tan, Y. Long, *Nano Energy* **2021**, *89*, 106440.
[29] W. Meng, Y. Gao, X. Hu, L. Tan, L. Li, G. Zhou, H. Yang, J. Wang, L. Jiang, *ACS Appl. Mater. Interfaces* **2022**, *14*, 28301.
[30] B. Li, F. Xu, T. Guan, Y. Li, J. Sun, *Adv. Mater.* **2023**, *35*, 2211456.
[31] H. Y. Lee, Y. Cai, S. Velioglu, C. Mu, C. J. Chang, Y. L. Chen, Y. Song, J. W. Chew, X. M. Hu, *Chem. Mater.* **2017**, *29*, 6947.
[32] Y. Feng, W. Ma, H. Li, M. Yang, Y. Yu, S. Liu, X. Zeng, F. Huang, Y. Yang, Z. Li, *ACS Appl. Mater. Interfaces* **2023**, *15*, 5836.
[33] R. Zhang, B. Xiang, Y. Shen, L. Xia, L. Xu, Q. Guan, S. Tang, *Busshitsu Kogaku Kogyo Gijutsu Kenkyusho Hokoku* **2021**, *9*, 17481.
[34] S. Zhao, Z. Shao, A. Huang, S. Bao, H. Luo, S. Ji, P. Jin, X. Cao, *Nano Energy* **2021**, *89*, 106297.
[35] Y. Cui, Y. Ke, C. Liu, Z. Chen, N. Wang, L. Zhang, Y. Zhou, S. Wang, Y. Gao, Y. Long, *Joule* **2018**, *2*, 1707.
[36] Z. Zhang, L. Zhang, Y. Zhou, Y. Cui, Z. Chen, Y. Liu, J. Li, Y. Long, Y. Gao, *Chem. Rev.* **2023**, *123*, 7025.
[37] Y. Zhu, Y. Yao, Z. Chen, Z. Zhang, P. Zhang, Z. Cheng, Y. Gao, *Sol. Energy Mater. Sol. Cells* **2022**, *239*, 111664.
[38] Y. Yang, J. Wang, D. Li, J. Yang, M. Fang, Z. Li, *Adv. Mater.* **2021**, *33*, 2104002.
[39] Y. Zhou, A. Huang, S. Ji, H. Zhou, P. Jin, R. Li, *Chem. - Asian J.* **2018**, *13*, 457.
[40] U. Joost, A. Sutka, M. Oja, K. Smits, N. Döbelin, A. Loot, M. Järvekülg, M. Hirsimäki, M. Valden, E. Nõmmiste, *Chem. Mater.* **2018**, *30*, 8968.
[41] S. Yamazaki, H. Ishida, D. Shimizu, K. Adachi, *ACS Appl. Mater. Interfaces* **2015**, *7*, 26326.
[42] S. Y. Chun, S. Park, S. I. Lee, H. D. Nguyen, K.-K. Lee, S. Hong, C.-H. Han, M. Cho, H.-K. Choi, K. Kwak, *Nano Energy* **2021**, *82*, 105721.
[43] T. T. Dao, S. Park, S. Sarwar, H. V. Tran, S. I. Lee, H. S. Park, S. H. Song, H. D. Nguyen, K.-K. Lee, C.-H. Han, S. Hong, *Sol. Energy Mater. Sol. Cells* **2021**, *231*, 111316.
[44] K. Adachi, M. Tokushige, K. Omata, S. Yamazaki, Y. Iwadate, *ACS Appl. Mater. Interfaces* **2016**, *8*, 14019.
[45] Y. Badour, S. Danto, C. Labrugère, M. Duttine, M. Gaudon, *J. Electron. Mater.* **2022**, *51*, 1555.
[46] T. Ma, B. Li, S. Tian, J. Qian, L. Zhou, Q. Liu, B. Liu, X. Zhao, G. Sankar, *Chem. Eng. J.* **2023**, *468*, 143587.
[47] K. Thummavichai, Y. Xia, Y. Zhu, *Prog. Mater. Sci.* **2017**, *88*, 281.
[48] Y. Zhou, N. Li, Y. Xin, X. Cao, S. Ji, P. Jin, *J. Mater. Chem. C* **2017**, *5*, 6251.
[49] J. Wei, X. Jiao, T. Wang, D. Chen, *J. Mater. Chem. A* **2018**, *6*, 14577.
[50] J. Wei, X. Jiao, T. Wang, D. Chen, *ACS Appl. Mater. Interfaces* **2016**, *8*, 29713.
[51] X. Dong, Z. Wu, Y. Guo, Y. Tong, X. Liu, L. Zhang, Y. Lu, *Sol. Energy Mater. Sol. Cells* **2021**, *219*, 110784.
[52] X. Cao, Z. Chen, R. Lin, W.-C. Cheong, S. Liu, J. Zhang, Q. Peng, C. Chen, T. Han, X. Tong, Y. Wang, R. Shen, W. Zhu, D. Wang, Y. Li, *Nat. Catal.* **2018**, *1*, 704.
[53] Y. Zhang, J. Zhao, H. Wang, B. Xiao, W. Zhang, X. Zhao, T. Lv, M. Thangamuthu, J. Zhang, Y. Guo, J. Ma, L. Lin, J. Tang, R. Huang, Q. Liu, *Nat. Commun.* **2022**, *13*, 58.
[54] G. W. Larson, R. A. Shakespeare, C. Ehrlich, J. Mardaljevic, E. Phillips. Rendering with Radiance: the art and science of lighting visualization, Morgan Kaufmann San Francisco, CA, USA, **1998**.
[55] A. Nabil, J. Mardaljevic, *Energy Build.* **2006**, *38*, 905.
[56] J. Wienold, J. Christoffersen, *Energy Build.* **2006**, *38*, 743.
[57] A. Mcneil, E. S. Lee, *J. Build. Perform. Simul.* **2013**, *6*, 24.
[58] E. Brembilla, J. Mardaljevic, *Build. Environ.* **2019**, *158*, 151.
[59] C. Pierson, J. Wienold, M. Bodart, *Buildings* **2018**, *8*, 94.

